Salisbury, M. H., Scott, J. H., et al., 1988
Proceedings of the Ocean Drilling Program, Scientific Results, Vol. 102

4. ELASTIC PROPERTIES OF 110-MA OCEANIC CRUST FROM SONIC FULL WAVEFORMS IN DSDP HOLE 418A[1]

Daniel Moos, Lamont-Doherty Geological Observatory, Palisades, New York[2]

ABSTRACT

Leg 102 of the Ocean Drilling Program reoccupied DSDP Hole 418A, drilled during DSDP Legs 51–53 to a total depth of 868 mbsf. The hole penetrates 544 m into the basalts of oceanic Layer 2. A full complement of geophysical logs was obtained during ODP Leg 102, including over 2000 digitally recorded 12-channel sonic full waveforms recorded over the interval from 469 to 788 mbsf. Compressional, shear, and Stoneley wave sonic velocities were calculated from the recorded waveforms using a modified semblance technique. The energy and frequency content of compressional and shear phases were computed from the optimal semblance windows. Compressional-wave velocities range from 4 to 6.4 km/s; shear-wave velocities range from 2 to 3.5 km/s. V_p/V_s is about 1.75 to 2.1. Elastic properties are different for different structural units: massive basalts have V_p/V_s below 1.8 and V_p above 5.8; pillows have quite variable velocities and V_p/V_s above 1.8; V_p/V_s is below 1.9 and V_p is above 5.8 in "massive" pillow Subunit 13B; breccia Subunit 6A has the lowest V_p and V_p/V_s of 1.9. These variations are due both to variations in crack aspect ratio and distribution and to variations in alteration. Velocities increase somewhat at the base of breccia Subunit 6B, and again at the Subunit 13A/Subunit 13B boundary. Otherwise velocities are independent of depth. Stoneley wave velocities increase from about 1.5 km/s above 411 mbsf to 1.6 km/s at the bottom of the logged interval. Maximum shear and compressional energy increases systematically with depth; as depth increases the basalts become more homogeneous. Scattering within pillows reduces the sonic peak frequency because of the similarity between the sonic wavelength and the size of pillows; peak frequency may be a sensitive indicator of lithology within the pillows and massive basalts of oceanic Layer 2. Stoneley wave velocities are higher in massive units and lowest in the Subunit 6A breccia; coherence of the Stoneley signal across the array is lower where porosities are higher, corresponding with intervals of poorer core recovery. Theoretical considerations suggest that this may be due to higher permeability within these intervals. If so, permeability within the upper crust appears to be concentrated within narrow zones rather than evenly distributed throughout the basement section.

INTRODUCTION

The elastic properties of most aggregate materials are controlled by the properties of the components and by their distribution (e.g., Wu, 1966; Kuster and Toksöz, 1974; O'Connell and Budiansky, 1974; Mavko and Nur, 1978). In oceanic basalts the primary components are basalt matrix, pore space, and alteration products replacing basalt and pores as the crust ages. In this simple system the relationship between the distribution of these components and the elastic properties of the aggregate, although complex, should be resolvable. Analyses of recovered core and *in-situ* measurements together yield estimates of the distribution and volume percentage of each component (e.g., Salisbury et al., 1980).

In general, measurements of properties such as elastic-wave velocity at different length scales (seismic, sonic, and ultrasonic) do not agree (e.g., Salisbury et al., 1985). The discrepancy between laboratory ultrasonic velocity of cores and *in-situ* seismic velocity can be explained by the presence of large-scale cracks, fractures, and voids not sampled in the cores. Simple porosity-velocity relationships such as Wyllie et al.'s (1958) time-average equation ($1/V_p = \phi/1.5 = (1 - \phi)/6.4$; ϕ = porosity) yield *in-situ* total porosities (ignoring the effect of alteration products) of 18%–35% for seismic Layer 2A, 4%–10% for seismic Layer 2B, and 2% or less for seismic Layer 2C, using Houtz and Ewing's (1976) layer velocity data and a "zero-porosity" velocity of 6.4 km/s. This simple relationship ignores the complexity of the pore-structure distribution and aspect ratio and the possible presence of alteration products. Sonic velocities often agree with seismic velocities within the inherent errors of the measurements (e.g., Salisbury et al., 1980), although in some cases large discrepancies are observed, such as the apparent absence of Layer 2A at Site 504 (Little and Stephen, 1985; Newmark et al., 1985). These differences can be reasonably ascribed to lateral heterogeneity, the limited resolving power of seismic experiments, or the inherent difficulty of obtaining accurate *in-situ* velocities in highly heterogeneous basalts using conventional sonic logs.

Careful analysis of the structure of oceanic basalts yields additional valuable information on the relationship between lithology and elastic properties. Direct observations of the wall of a core hole using the borehole televiewer (Anderson and Zoback, 1983; Hickman et al., 1984; Newmark et al., 1985) and of the recovered cores differentiate between pillows, massive basalts, and breccias. The structural variations are also accompanied by differences in the elastic properties of these units. For example, Moos et al. (1985a) found that sonic compressional- and shear elastic-wave velocities and their ratio are quite different for pillows, massive units, and their fractured equivalents. These differences were ascribed to differences in the distribution and aspect ratio of the large-scale porosity.

Complicating this simple picture is the fact that both the size of pillows and the fracture spacing are typically on the order of the wavelength of the sonic energy; thus, simple models for aggregate materials are not generally applicable. The scattering properties of the aggregate often dominate when the elastic wavelength is about the same as that of the heterogeneities (Kikuchi, 1981; Frankel and Clayton, 1986). Sonic measurements, because of the similarity between the wavelength and the size of the heterogeneities, are most strongly affected and therefore most helpful in characterizing the large-scale porosity.

[1] Salisbury, M. H., Scott, J. H., et al., 1988. *Proc. ODP, Sci. Results*, 102: College Station, TX (Ocean Drilling Program).

[2] Addresses: Borehole Research Group, Lamont-Doherty Geological Observatory, Palisades, NY 10964; (Present address) Department of Geophysics, Stanford University, Stanford, CA 94305.

This paper presents the results of high-resolution full waveform sonic logs run in DSDP Hole 418A during ODP Leg 102. A full complement of Schlumberger logs was also recorded in the hole (Broglia and Moos, this volume), as was an oblique seismic experiment (Swift et al., this volume). These data, combined with the high core recovery, provide a unique opportunity to understand in detail the effects of structure, porosity, and alteration on the propagation of elastic waves in the oceanic crust.

PHYSICAL PROPERTIES FROM LOGS AND CORES

Core recovery in Hole 418A during DSDP Legs 52 and 53 averaged 72% (Donnelly, Francheteau, et al., 1980). The core recovery is shown in Figure 1, along with lithostratigraphy inferred from the recovered material. Recovery within massive units is typically higher than the average; recovery within pillows and within the breccia of Subunit 6A is somewhat lower. This is not surprising and in particular, may lead to a slight underestimation of the volume of pillows or breccias *in situ* (note that Core 418A-39, which may have contained some of the breccia unit, has less than 20% recovery). Basaltic composition within the cored interval is quite uniform. The basalts are porphyritic, with plagioclase the dominant phenocryst, olivine, and minor amounts of spinel. Alteration is predominantly due to low-temperature interaction with seawater and increases potassium and hydroxyl content, adding smectite, calcite, pyrite, and zeolites primarily as veins and vesicle fillings, but also replacing olivine and interstitial groundmass. Smectite content within the cores is quite high in the pillows of Unit 5 and the breccia Subunit 6A and is much lower in the remainder of the hole. The shipboard visual alteration index (shown as hachured marks in the core logs) decreases below Subunit 6A, although a few zones within pillow Subunit 6B are somewhat altered. The physical properties of the recovered cores are discussed in detail in the Leg 51–53 *Initial Reports* (Donnelly, Francheteau, et al., 1980). Ultrasonic velocity and core bulk density and porosity are also reviewed in Broglia and Moos (this volume). Typically, ultrasonic velocities in the freshest basalt cores range from 5.6 to 6.4 km/s, porosities range from 2% to 8%, and bulk densities range from 2.75 to 2.95 g/cm^3. Cores containing small amounts of alteration products typically have lower densities and velocities and higher porosities. There is no apparent difference between the properties of "fresh" massive basalts and "fresh" pillows.

Gamma-gamma density, neutron porosity, resistivity, sonic compressional-wave velocity, and natural gamma radiation logs were run from 478 m below seafloor (mbsf) (154 m into basement) to total logged depth (789 mbsf, 465 m into basement), and velocity, resistivity, and gamma-ray logs were also obtained in the upper part of the hole. The results, after correction for environmental effects and core calibrations, are also presented in Figure 1. Resistivity is plotted on a logarithmic scale, and compressional velocity and bulk density are plotted linearly. The porosity is divided into the volumetric contributions of basalt matrix, primary or microcrack porosity (which can be sampled by coring), fracture porosity (the portion of the porosity that cannot be sampled), and smectite (determined from the comparison of the recovered smectite volume and the gamma-ray log potassium yield). The data have been smoothed using a 5-m running average to emphasize trends.

Primary or microcrack porosity decreases systematically with increasing depth from about 15% in the uppermost section to less than 5% in the bottom of the logged interval. Fracture porosity is less than 10% throughout much of the hole, decreasing to zero in massive units (e.g., Unit 10), although the averaging scheme tends to smear the layer boundaries somewhat. Total porosity is as high as 25% in some portions of the Unit 5 pillow basalt. The smectite content matches the trends inferred from core recovery. No smectites are found in the massive units, and below the Subunit 6A breccia, smectite content in the pillows is below 5%. However, in Unit 5 and Subunit 6A smectite content ranges from 10% to more than 20%. Broglia and Moos (this volume) found somewhat higher porosities in Hole 418A than Salisbury et al. (1980) found in Hole 417D. It is interesting to note that the latter's best-fit velocity-porosity relationship is the Wyllie time-average equation (Wyllie et al., 1958), whereas the former's data are fitted best by a volume average of the velocity. The time-average equation assumes that the components are arranged as layers across which the elastic wave traverses, sampling each component according to its volume percentage, and thus yields minimum values of velocity for a given percentage of slow components. The volume average is closer to Hyndman et al.'s (1984) velocity-porosity relationship based on core data and yields higher values of velocity for the same component distribution. Thus, the porosities obtained by Broglia and Moos (this volume) fit their linear relationship, whereas the lower porosities of Salisbury et al. (1980) fit the time-average equation. A recent study of clay-bearing sandstones indicates that the best-fitting component relationship is a volume average of the velocities (Han et al., 1986).

From these results it is reasonable to consider the uppermost 500 m of basement at Site 418 to be a three-phase (water-basalt-smectite) system; up to a few percent interpillow limestone (which has a matrix velocity close to that of the basalt) is also present in some sections. Grain-boundary or microcrack porosity is 0% to 20%, fracture porosity ranges from 0% and 20%, and smectite content is between 0% and 25% by volume.

THE MULTICHANNEL SONIC LOG

The multichannel sonic (MCS) logging tool deployed during Leg 102 in Hole 418A is a modification of the device used by Moos et al. (1985a). The logging sonde consists of a magnetostrictive source separated from a set of 12 piezoelectric receivers by a 1-m acoustic isolator section. The receivers are spaced at 0.15-m intervals within an oil-filled hydraulic hose, forming a 1.65-m array. The first receiver is separated from the source by 1.95 m. The sonde is centered in the hole by two sets of bow-spring centralizers, one located above the source and one below the receivers. Acoustic energy is emitted by the source, propagates through the fluid-filled hole, and generates a series of waves refracted along the borehole wall as well as a set of borehole modes. Cheng and Toksöz (1981) and Paillet and White (1982) discuss the theory of acoustic-wave propagation in boreholes. The first energy arriving at the receivers is a refracted compressional wave, followed by a refracted shear wave, if the formation shear-wave velocity is higher than the propagation velocity of acoustic energy in the fluid. Following the shear wave is the first normal mode, or pseudo-Rayleigh wave. Higher order modes are seen only if the source generates energy above their low-frequency cutoff. The Stoneley wave, which is evanescent in both the fluid and formation, propagates at slightly less than the acoustic-wave velocity in the fluid. Its characteristics are controlled by the properties of the borehole wall and by the permeability of the formation (e.g., Rosenbaum, 1974; Paillet, 1983; Hsui et al., 1985), in addition to the velocities, densities, and attenuating properties of the formation and fluid. Figure 2 is a schematic of the MCS sonde and shows waveforms recorded in a hole drilled through granodiorite, in which each of the phases can be seen.

Data

The MCS data were recorded from just above the bottom of the hole at 789 mbsf to just above a bridge at 464 mbsf. The uppermost 140 m of basement were not logged. Figure 3 presents the waveforms recorded at receiver 4, 2.4 m below the source. The data can be thought of as a constant-offset sonic "section," geometrically similar to a seismic-refraction section, of the ma-

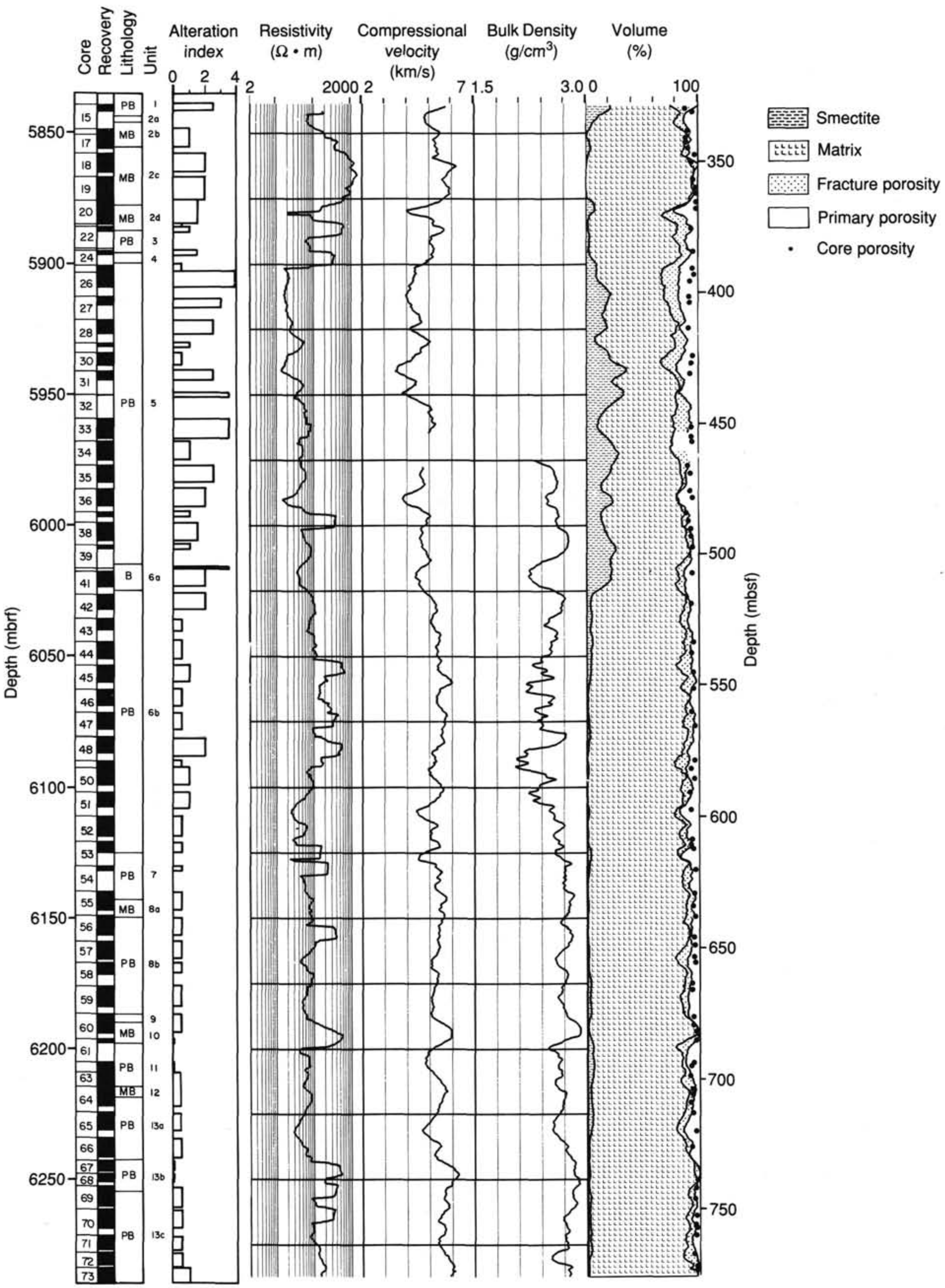

Figure 1. Summary of core descriptions and log physical properties in the basement section of DSDP Hole 418A. Core properties at left are recovery, inferred lithology (PB = pillow basalt; MB = massive basalt; B = breccia), and visual alteration index. Log properties are resistivity, sonic compressional-wave velocity, bulk density, and the volume percentages of alteration clay minerals (smectite), basalt, fracture (large-scale) porosity, and primary (vesicular and/or intergranular) porosity. The log data are averaged over 5-m intervals. After Broglia and Moos (this volume).

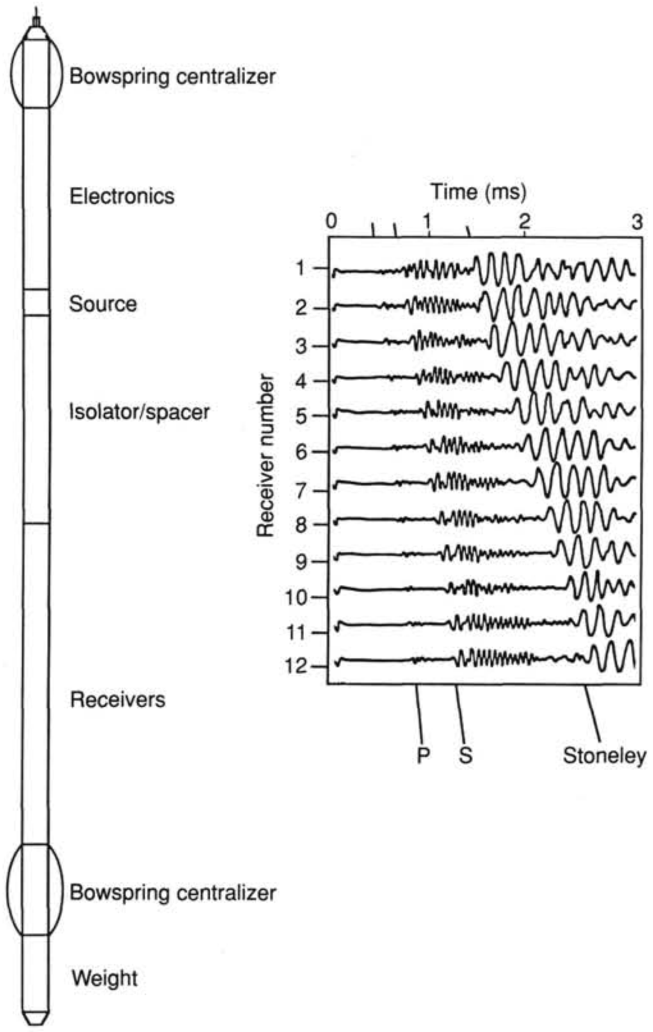

Figure 2. Schematic of the multichannel sonic logging tool and a sample waveform suite showing arrivals in a granodiorite (V_p = 6.3 km/s; V_s = 3.6 km/s).

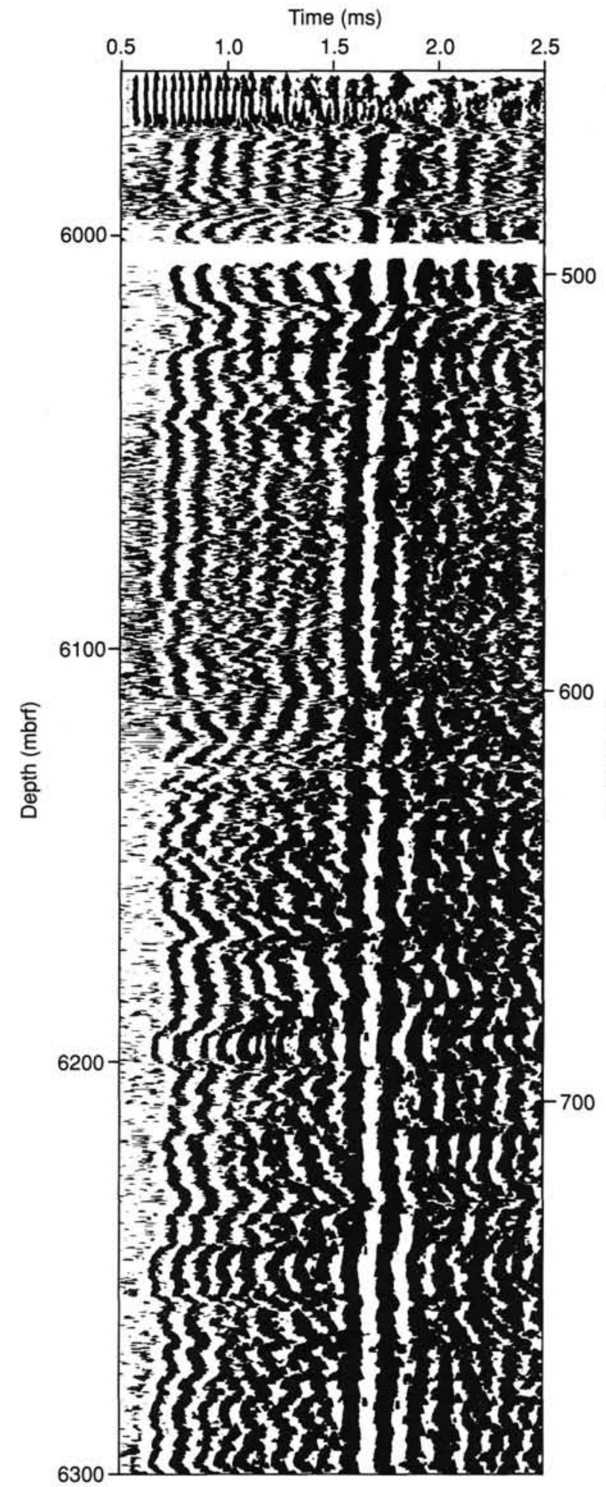

Figure 3. Full waveforms recorded in DSDP Hole 418A at receiver 4, 2.4 m below the source. Variations in arrival time are a function both of changes in velocities and changes in hole size. Depth in m below seafloor (mbsf) and m below rig floor (mbrf). No data were recorded in the interval between 489 and 499 mbsf.

terial penetrated by Hole 418A. Variations in the character and arrival time of the different phases are due to changes in hole size and rock properties. The first arrival is the refracted compressional wave. The low-frequency constant arrival-time phase at about 1.7 ms is the Stoneley wave. The shear wave can be seen clearly in the lowermost 50 m of the hole and within massive units (for instance, Units 9 and 10 at 676–686.5 mbsf). Its arrival time, shortly after the compressional first break, varies in the same sense but more than the compressional arrival, as the elastic properties of the formation change.

The variations in amplitude, velocity, and frequency content of these arrivals can be seen more clearly in "gathers" of the data recorded at each of the 12 receivers at a given source depth. Figures 4A–4H show typical suites of data recorded within each unit. The first observation is that these data are much less coherent and generally have lower frequencies than the data recorded within granodiorite (Fig. 2). However, frequency variations exist even within the data from Hole 418A. Each of the arrivals seen in Figure 2 can be identified here as well.

Figure 4A was recorded within massive Unit 10 at 684 mbsf. Compressional, shear, and Stoneley arrivals can be identified across the receiver array. The compressional arrival is quite high in frequency; the shear arrival is lower in frequency and is followed by a high-frequency phase tentatively identified as the first normal mode. The Stoneley arrival has a much lower frequency and is sustained for more than 1.5 ms.

Figure 4B was recorded within massive pillow Subunit 13B at 738 mbsf. Although strong compressional and Stoneley arrivals are seen, the shear arrival is somewhat obscured. The frequency

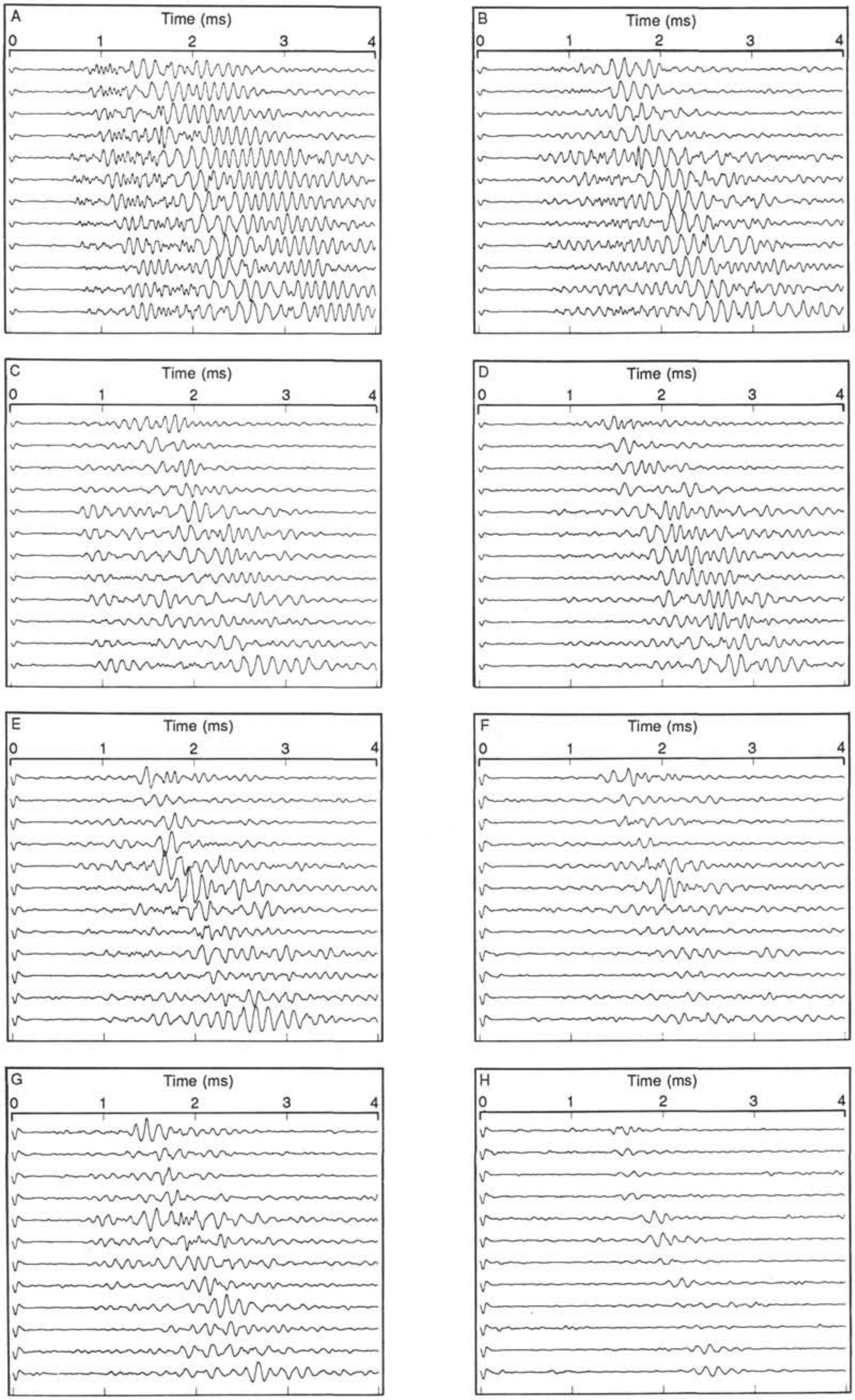

Figure 4. Waveform suites at selected intervals in DSDP Hole 418A showing variations in amplitude and frequency content for the different units: A. 684 mbsf, massive Unit 10; B. 738 mbsf, massive pillow Subunit 13B; C. 764 mbsf, pillow Subunit 13C; D. 699 mbsf, pillow Unit 11; E. 549 mbsf, pillow Subunit 6B; F. 584 mbsf, pillow Subunit 6B; G. 509 mbsf, breccia Subunit 6A; H. 484 mbsf, across a bridge within pillow Unit 5.

content of the compressional arrival is lower than in Figure 4A; however, the high-frequency post-shear phase is present. The Stoneley arrival is much less sustained.

Figure 4C was recorded within pillow Subunit 13C at 764 mbsf. The Stoneley amplitude is significantly reduced and although compressional and shear phases are observed, they contain no high frequencies.

Figure 4D was recorded within pillow basalt Unit 11 at 699 mbsf. No shear wave is apparent in these records, and the compressional wave is low in frequency and of short duration. The Stoneley wave is still present, however. Figures 4E and 4F were recorded in a similar lithology at shallower depths (549 and 589 mbsf, respectively) within pillow Subunit 6B, and compressional and Stoneley waves are further degraded. These figures are displayed with a 2× gain factor because the signal amplitude is significantly lower than that recorded at 699 mbsf.

Figure 4G was recorded within breccia Subunit 6A. Although its features are quite similar to those of Figures 4D–4F, the Stoneley wave is quite incoherent, and the amplitude of the compressional wave varies across the receiver string. This figure is also displayed with a 2× gain factor.

Figure 4H was recorded within a bridged interval, or constriction, at 484 mbsf. No coherent refracted energy is seen in this section; similarly, the entire zone between 486 and 478 mbsf on Figure 3 contains little energy. However, there is a low-amplitude Stoneley wave present in the record at 484 mbsf.

The differences apparent in Figures 4A–4H can be attributed both to lithologic differences and to environmental effects such as hole size changes or well bore roughness. Note that higher frequencies are observed in data from massive units and that energy content and coherence increase with increasing depth within pillows. The absence of a significant component of refracted energy at 484 mbsf is most likely due to the affect of the bridge, although the presence of a bridge at that depth presumably results from a change in the properties of the formation. Although variations in well bore roughness related to changes in the degree of infilling and alteration probably occur, the remainder of the well is essentially to gauge. Thus, these variations are due to changes in the intrinsic properties of the basalts. Analyses of the full sonic wave train, described in the next section, quantify these effects and allow us to study the variations in velocity, amplitude, and frequency of the compressional, shear, and Stoneley waves as a function of lithology and depth.

Analysis

The velocities of compressional, shear, and Stoneley waves are calculated using a modified semblance technique. This technique has been employed by a variety of researchers to analyze sonic waveforms (e.g., Kimball and Marzetta, 1984; Goldberg et al., 1984; Moos et al., 1985b). Semblance is a measure of the coherence of a signal across an array of receivers and is defined as the sum of the cross-correlations at a fixed lag proportional to the receiver offset divided by the sum of the autocorrelations of each received signal. Semblance varies between 0 and 1, where 1 is perfect coherence and 0 is a perfectly random signal. The semblance for a given arrival will be highest when the lag at each receiver is the product of the slowness (inverse velocity) and the offset. The technique employed here computes semblance across the receiver array of a narrow time window of the data. The typical window length is 200 μs, or about two full cycles of a 10-kHz signal. The start time of the window varies, depending on which arrival is being studied. To determine the propagation velocity of a discrete phase, the window is fixed by selecting a start time at the first receiver. Alternatively, the start time can be fixed at the source to study the entire wave train in a single pass.

Figure 5 shows a typical semblance "path" through the data. Note that the window shown here is that used to compute energies and peak frequencies and is different from the semblance window just described. Figure 6A is a semblance panel for the data shown in Figure 4A. Here the semblance value is plotted on a gray scale, with higher semblance generally a darker gray. The x-axis is slowness; the y-axis is the start time of the window at the first receiver. The first arrival from 400 to 800 μs is the compressional wave (*P*); its slowness is about 54 μs/ft, corresponding to a velocity of 5.64 km/s. The arrival is quite ringy, indicating the presence of large amounts of "leaky P" energy, but the slowness is constant; the *P*-wave is essentially nondispersive. The next arrival is the shear wave (*S*). Its slowness is about 94 μs/ft, corresponding to a velocity of 3.24 km/s; the V_p/V_s ratio is 1.74. Again, the arrival is quite ringy. Here, however, the later portion is somewhat slower than the initial arrival—evidence of the presence of the first normal mode or pseudo-Rayleigh wave. The Stoneley wave arrives later in the wave train with a slowness of about 195 μs/ft. Its velocity of 1.56 km/s is only slightly less than the acoustic velocity of the borehole fluid at the appropriate temperatures and pressures, as expected. The magnitude of the semblance is above 0.8 for all three arrivals.

Figures 6B–6G show similar semblance calculations for the waveforms shown in Figures 4B–4G. The relative coherence of each arrival within these waveform suites is quite clearly reproduced by the magnitude of the associated semblance maximum. For example, the absence of any coherent direct arrival in Figure 4G results in a very low semblance for the *P*-wave (less than 0.5) and no semblance maximum for the *S*-wave, although the Stoneley arrival is observed. Note also that the velocity of the Stoneley wave varies with lithology, suggesting that it is sensitive to subtle structural differences between pillows and flows.

By fixing the window start time at the source, rather than at the first receiver, one can calculate in a single pass the semblance as a function of slowness for each depth. Figure 7 shows

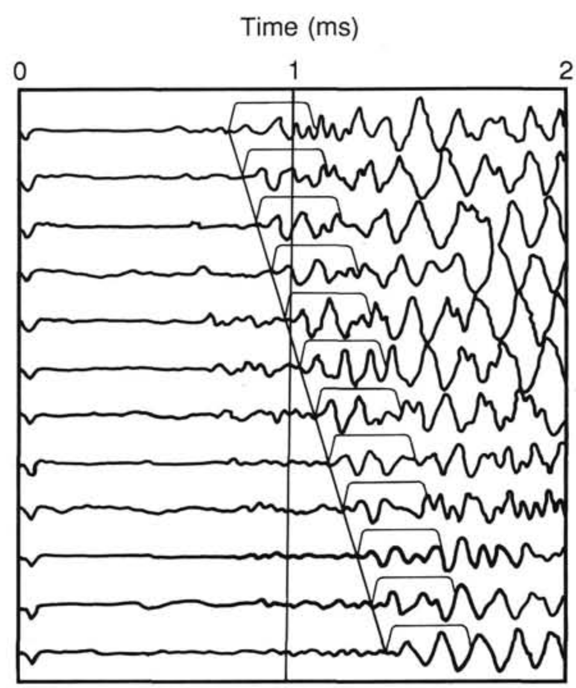

Figure 5. Semblance window centered on the shear arrival at 628 mbsf. Amplitudes and frequencies were computed using the semblance arrival times and the 300-μs window shown. The semblance velocities were calculated using a 200-μs window with the same start time.

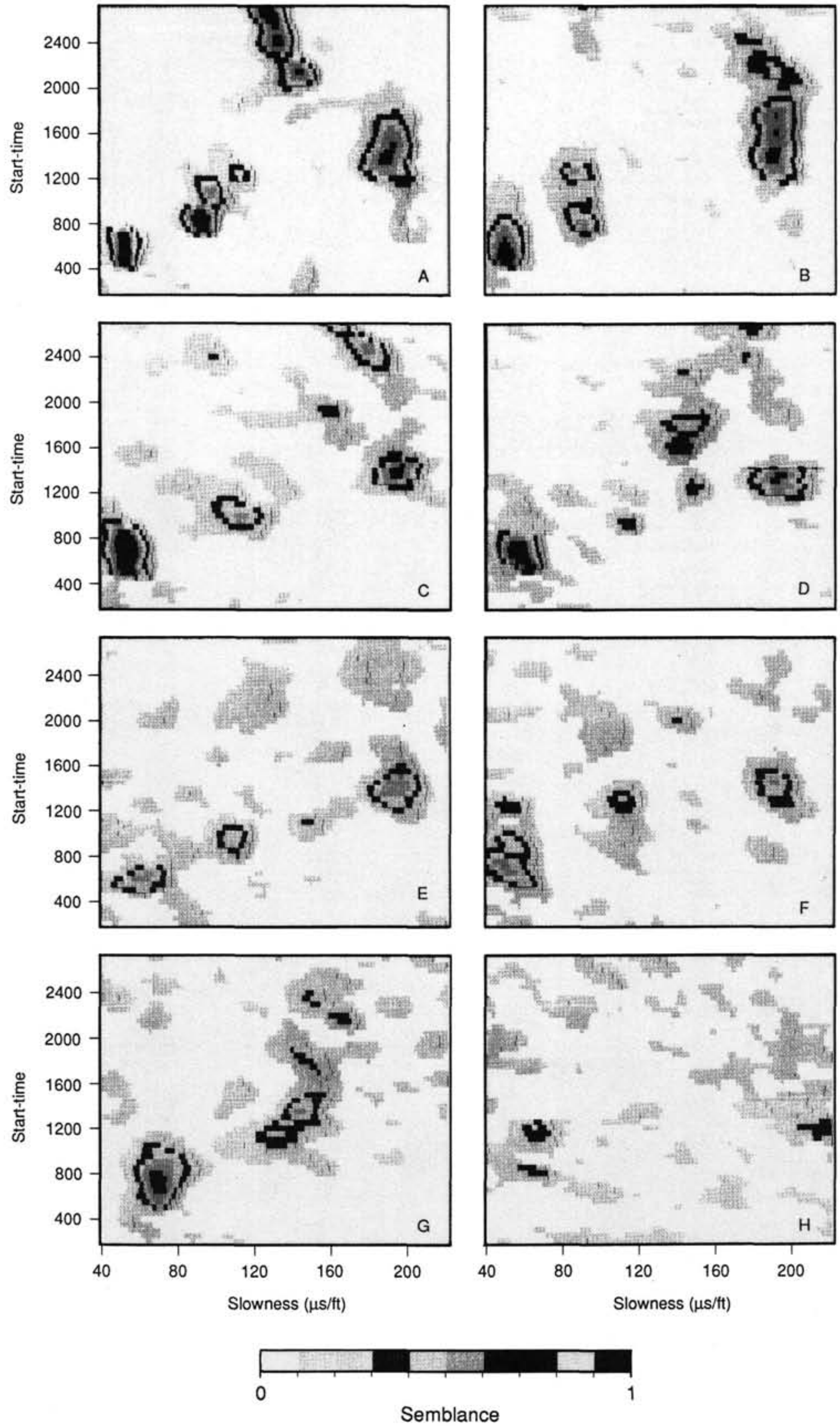

Figure 6. Semblance panels for the data in Figure 5. The y-axis is the start time of the window at the first receiver in μs (roughly equal to arrival time). The x-axis is slowness (inverse velocity). A. 684 mbsf, massive Unit 10. B. 738 mbsf, massive pillow Subunit 13B. C. 764 mbsf, pillow Subunit 13C. D. 699 mbsf, pillow Unit 11. E. 549 mbsf, pillow Subunit 6B. F. 584 mbsf, pillow Subunit 6B. G. 509 mbsf, breccia Subunit 6A. H. 484 mbsf, across a bridge within pillow Unit 5.

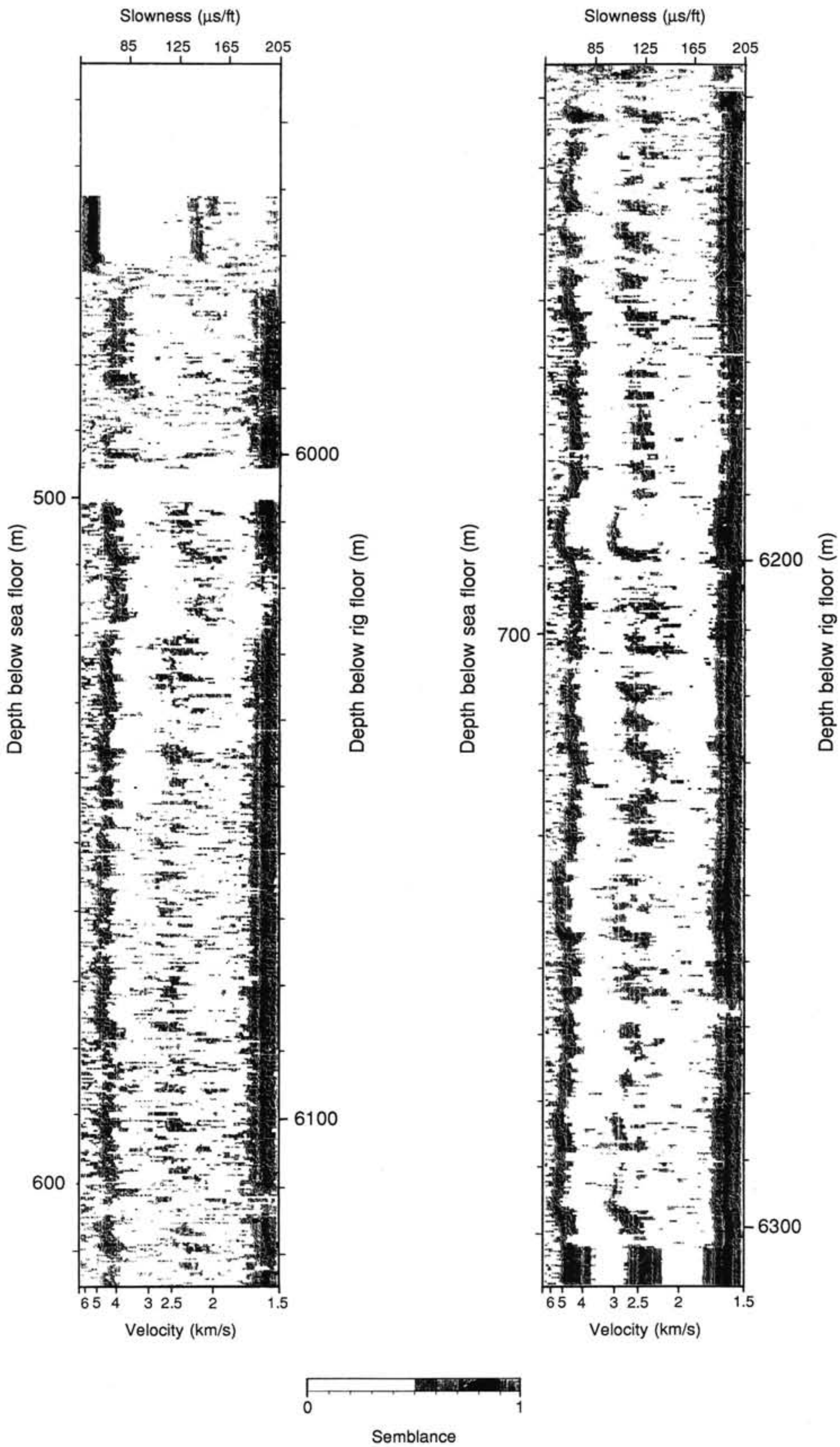

Figure 7. Semblance as a function of depth and slowness (inverse velocity) for Hole 418A. Peaks correspond to compressional, shear, and Stoneley arrivals. Slowness ranges from 40 to 200 μs/ft, corresponding to a velocity range from 7.62 to 1.524 km/s. Typically, compressional energy travels at 50 to 70 μs/ft (6.10 to 4.35 km/s), and shear energy travels at 85 to 110 μs/ft (3.59 to 2.77 km/s). The Stoneley arrival travels at 185 to 200 μs/ft (1.524 to 1.65 km/s). Variations in intensity indicate changes in semblance amplitude (and hence the coherence of the arrival).

semblance as a function of slowness and depth for the entire logged interval. Slowness ranges from 40 to 200 μs/ft, to include compressional, shear, and Stoneley arrivals. Comparison of these results to the full waveforms (Fig. 3), waveform suites (Fig. 4), and semblance panels (Fig. 6) provides insight into the effects of lithology on borehole waveforms and thus, yields additional information on the properties of the formation. Variations in lithology affect both the velocity and semblance value for the sonic waves. For instance, massive basalt Units 9 and 10 (676–687 mbsf) are characterized by high velocities (low slownesses) and high semblances. Breccia Subunit 6A (504–514 mbsf) has low velocities and low semblance, indicating low coherence. Semblances are quite low in smectite-filled Unit 5, particularly the interval around 469 mbsf where density and resistivity are low (Fig. 1). Pillows have variable velocities and generally lower semblances. The method employed here works best when the hole size is invariant. Thus, part of the semblance variation is due to changes in hole size that result in variations in the arrival time of the different phases, causing the arrivals to move out of the optimum window for the semblance calculation.

Using slowness windows determined from the results displayed in Figure 7, more precise calculations of compressional, shear, and Stoneley wave velocities can be made. Figure 8 shows the results of these calculations and the velocity ratio V_p/V_s. Also shown in Figure 8 is the magnitude of the semblance for each phase. This is related to the coherence of the arrival and thus, to the heterogeneity of the formation. V_p and V_s show relatively little systematic increase with depth. V_p varies between 4 and 6.4 km/s, and V_s varies similarly between 2 and 3.5 km/s. V_p/V_s generally ranges from 1.75 to 2.1. Small, stepwise velocity increases occur at the base of the Subunit 6A breccia (514 mbsf) and at the Subunit 13A (pillow basalt)/Subunit 13B (massive pillow) boundary at 731.5 mbsf. Stoneley velocity is between 1.5 and 1.6 km/s and shows a systematic increase from 459 to about 569 mbsf, below which it is relatively constant. As one might expect, velocities are highest in massive basalts and lowest in the basalt breccia; V_p/V_s is lowest in massive units and higher in pillows. Physical properties are more variable in pillow units, particularly between 569 and 629 mbsf, where the caliper log indicated poorer hole conditions (Broglia and Moos, this volume), and above 489 mbsf in the more altered material above the Subunit 6A breccia.

One consequence of the semblance computation is the simultaneous measurement of waveform coherence. Although difficult to quantify, this measurement can be used both as a quality indicator and as an indication of formation heterogeneity. In general, one would expect shear semblance to be somewhat lower than compressional semblance owing to "leaky P" reverberations that interfere with the shear arrival. Furthermore, one might expect for each arrival that semblance within massive units would be higher than in pillows and that semblance would be lowest where poor hole conditions predominate. Stoneley semblance should be quite high, owing to the strong, coherent nature of this arrival. The data essentially confirm these expectations. Stoneley semblance is above 0.7 throughout the logged interval. Low semblance occurs within the Subunit 6A breccia (504–514 mbsf), within Subunit 13C Core 418A-70 (770 mbsf), and intermittently within the pillow units in the remainder of the hole. Compressional semblance is lowest above 489 mbsf, intermittently low within the Subunit 6B pillow basalt, and highest in massive units and toward the bottom of the hole. Similar results are seen for shear semblance, but its magnitude is lower and much more sensitive to heterogeneities.

Once the semblance calculations have been completed, one can use the optimum windows to isolate individual arrivals and study variations in energy and frequency content. Figure 5 shows the window employed to determine these quantities. The window is a 300-μs boxcar with a sinusoidal taper over the outer 30 μs. The same window was used for both compressional and shear arrivals. The energy within each window was measured by integrating the spectral amplitudes computed with a fast Fourier transform (FFT) that are within the 5- to 25-kHz frequency band. The peak frequency is simply the frequency for which the spectral amplitude within this window is greatest.

Figure 9 shows the results of this analysis. Plotted are compressional and shear energies and peak frequencies for receivers 6 and 8, 2.65 and 2.95 m away from the source. The *P*- and *S*-wave energies for a given receiver correlate quite well, as do the *P*- and *S*-wave frequencies. Similarly, the peak frequency and the integrated energy for *P* at the two receivers also correlate. Looking at the compressional frequency curves (PF6 and PF8), one can see a strong correlation between lithology and peak frequency. This was also observable in the waveform data shown in Figure 4. Units identified as massive in the cores are characterized by a significant increase in high frequencies for the compressional wave. The peak frequency within pillow units varies between 6 and 10 kHz, whereas in massive units the peak frequency is as high as 15–20 kHz. This correlation is not seen as strongly in the shear data, where the peak frequency varies between 5 and 10 kHz. In general, the shear peak frequency is lower than the compressional peak frequency. The relationship between energy and lithology is much less clear, although energy content increases somewhat with depth.

Discussion

The foregoing analyses provide compressional and shear velocities, peak frequencies, and energies for signals propagated along the wall of the core hole as a function of depth. The obvious relationships for these data are (1) high velocities and low velocity ratios in massive units, along with higher coherence and more high frequencies; and (2) lower coherence, more variable velocities, higher ratios, and lower frequencies in pillows, especially where the core hole wall is rough. There is no systematic increase in frequency content with depth for either shear or compressional waves. However, energy content increases toward the bottom of the well. In particular, the magnitude of the semblance increases with depth, indicating that there is more correlatable energy at deeper levels. This is primarily the result of changes in the scattering characteristics of the basalts and may be related to an increase in cementation of the pillows or the presence of more massive units at greater depths. Differences between energy and frequency content for material above and below the Subunit 6A breccia are quite small, although coherence decreases somewhat above this unit.

Compressional and shear sonic waves at these frequencies (5–20 kHz) generally have wavelengths between 0.1 and 1 m. This is at the lower end of the size range for pillows in these basalts (e.g., Donnelly, Francheteau, et al., 1980). The variations in frequency and energy for shear and compressional waves between pillows and massive units could therefore be a function of their structural differences, particularly because the size of the pillows is within an order of magnitude of the wavelength of the dominant sonic energy. Anderson et al. (1985) observed similar results in Hole 504B and attempted to explain them by an acoustical "venting" mechanism.

A somewhat simpler alternative explanation is related to the fortuitous coincidence between pillow size and sonic wavelength. Scattering of elastic-wave energy is a function of the relationship between the wavelength and the size of the scatterers (e.g., Aki and Richards, 1980; Frankel and Clayton, 1986). In general, the attenuation due to scattering is greatest when the wavelength is close to the size of the scatterers. Frankel and Clayton (1986) found that the maximum energy loss occurs when the ratio a/λ is between 1 and 2. Here a is the correlation distance between the scatterers and λ is the sonic wavelength. The energy loss also depends on the heterogeneity of the material. In this

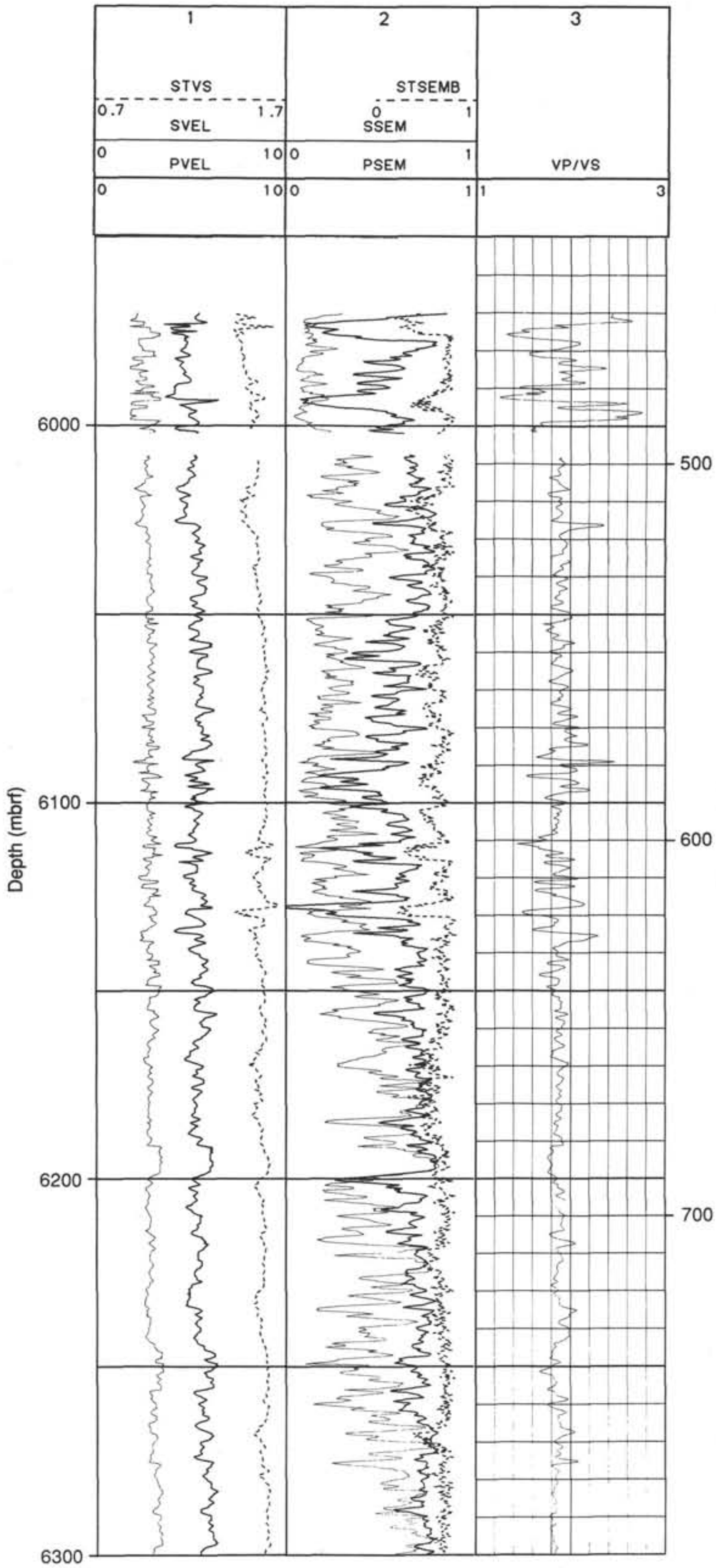

Figure 8. Compressional- (PVEL) and shear- (SVEL) wave velocities and V_p/V_s (VP/VS) for Hole 418A, compressional (PSEM) and shear (SSEM) semblances, and Stoneley velocity (STVS) and semblance (STSEMB) as a function of depth in Hole 418A. No data were recorded between 489–499 mbsf. Data were averaged over 1.5-m intervals. Semblance varies between 0 and 1, where 1 is perfect coherence. Decreased semblance is due to loss of energy of the primary arrival by scattering or intrinsic attenuation or from interference from secondary phases within the semblance window. Velocities in km/s.

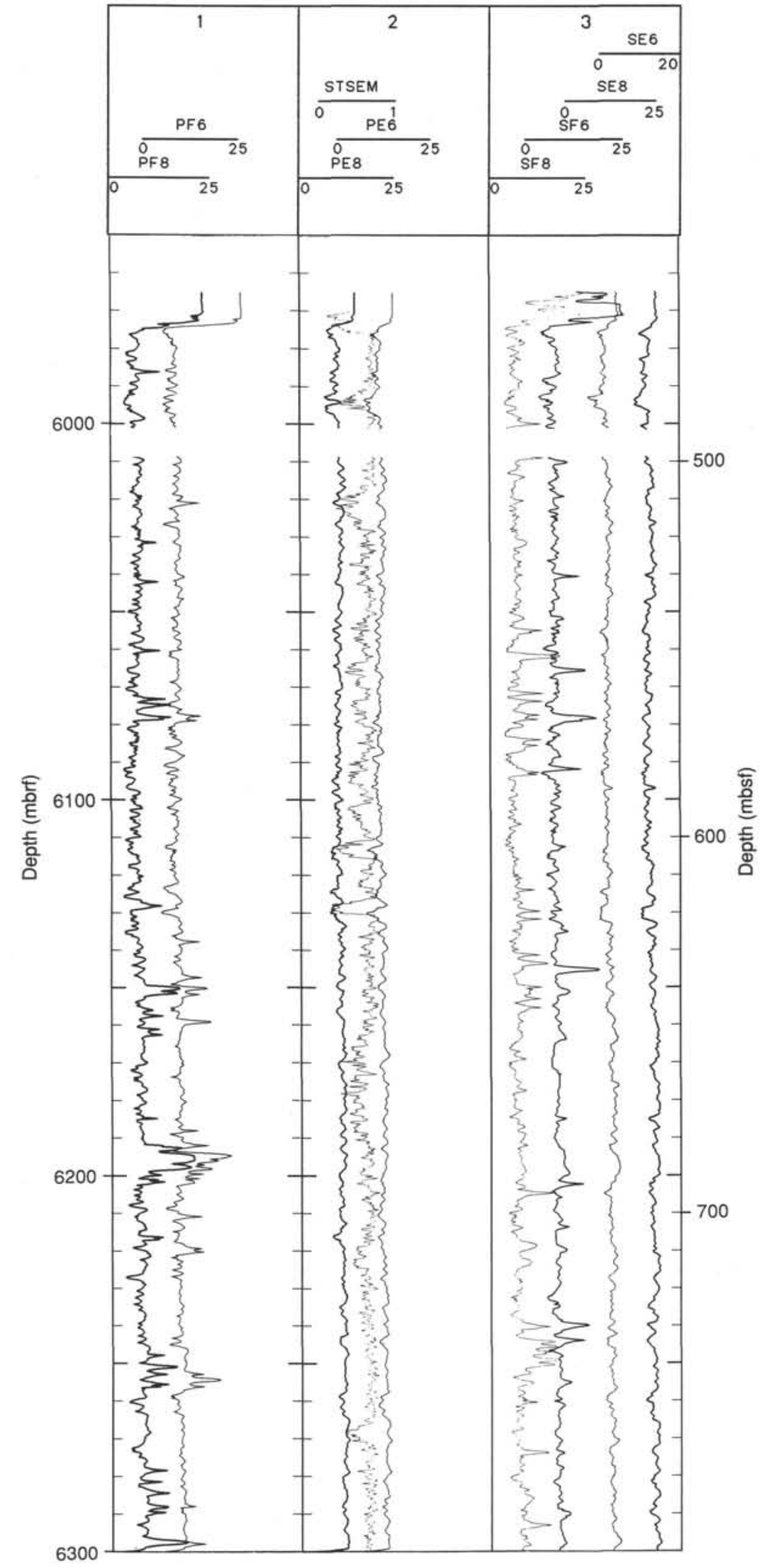

Figure 9. Peak frequency (F, in Hz) and energy (E, in dB) plots for P (P) and S (S) waves at receivers 6 and 8, with Stoneley semblance (STSEM) as a function of depth in Hole 418A. Higher peak frequencies occur within massive Subunit 8A (632–636 mbsf), Unit 9 (676–679 mbsf), Unit 10 (679–686.5 mbsf), and massive pillow Subunit 13B (731.5–743.8 mbsf). Higher peak frequencies are also measured in short sections not identified as massive units from core descriptions (e.g., within Subunit 13C below 744 mbsf). Peak energy increases somewhat with increasing depth.

case the amount of scattering depends on pillow size, sonic wavelength, and the difference between the properties of the pillows and the interstitial material. The relationship between velocity (v), frequency (f), and wavelength (λ) is $\lambda = v/f$. Using this relationship, one can estimate the size of the pillows from the observed sonic-wave spectra, with the assumption that the spectrum is a consequence of scattering losses within the pillows.

Figure 10 shows the frequency spectrum for shear and compressional waves recorded within the massive basalt Unit 10. The waveforms are windowed as shown in Figure 5, and the spectra are computed by an FFT; power is plotted on a logarithmic scale as a function of frequency. The compressional-wave spectrum is sharply peaked, with maxima at 4, 8.5, and 22 kHz. The shear-wave peaks are at 6.5, 10.5, and 19 kHz, respectively. In contrast, the spectrum for waves within pillow Subunit 8B has little energy above 10 kHz. The position of the energy minimum at about 16 kHz for *P*-waves and 11–12 kHz for *S*-waves does not change with lithology. The strongly peaked appearance of the power spectrum is caused by the propagation characteristics of the borehole environment and is not due to artifacts of the processing technique (Paillet, 1981).

The wavelength corresponding to the compressional peak at 22 kHz is about 0.23 m, assuming a velocity in the pillows of 5.0 km/s. The shear peak at 19 kHz has a wavelength of about 0.13 m, assuming a velocity of 2.5 km/s. The loss of energy at high frequencies for *P*- and *S*-waves within the pillow section indicates that energy within the wavelength range around 0.23 m for *P*-waves and 0.13 m for *S*-waves is scattered within the pillows and not within the massive unit. Thus, the optimum size for scattering is somewhat less than 0.25 m. The observation that compressional energy is a better discriminator than shear energy (Fig. 10) implies that the size is larger than optimum for shear waves at this frequency and is consistent with a scattering radius greater than 0.25 m, within the size range for pillows in these basalts (Donnelly, Francheteau, et al., 1980). Although the propagation distances are on the order of 1 to 2 m (5–10 wavelengths), the energy in the higher frequency lobe is reduced by more than 10 dB compared to that in the lower frequency lobe. This large energy loss for wavelengths within the range of the pillow size suggests that the pillows themselves are quite efficient scatterers of sonic energy.

Compressional and shear velocities calculated from the full waveform data provide a unique opportunity to observe the variation in V_p, V_s, and V_p/V_s within 110-Ma crust and to compare these parameters to lithologic and structural variations and to depth. A similar exercise in DSDP Hole 504B revealed systematic differences within young (<6 Ma) oceanic basalts of Layer 2A (Moos et al., 1985a). Figure 11 is a plot of V_p vs. V_p/V_s for depths where compressional and shear semblances are above 0.4. This eliminates the most heterogeneous intervals throughout the well and probably removes some valid data. However, variations between structural units are preserved.

The shaded areas in Figure 11 correspond to the range of values in massive basalts (Subunit 8B and Units 9, 10, and 12), massive pillows (Subunit 13B), breccias (Subunit 6A), and pillows. Data in the pillows is further differentiated by depth: above 611 mbsf (Unit 5 and Subunit 6B), 611–704 mbsf (Units 7 and 11 and Subunits 8A and 8C), and below 707 mbsf (Subunits 13A and 13C). Breccias exhibit the lowest compressional velocities and very consistent V_p/V_s of 1.9. Massive units have the lowest V_p/V_s (<1.82) and compressional velocities between 5.8 and 6.4. Pillows have quite variable compressional velocities (from 4.7 to more than 6 km/s) and V_p/V_s above 1.8. Massive pillows have compressional velocities above 5.8. There is no systematic increase in the range of compressional velocities with increasing depth in the pillows, although higher velocities and lower V_p/V_s are observed in the deeper sections. Note that the

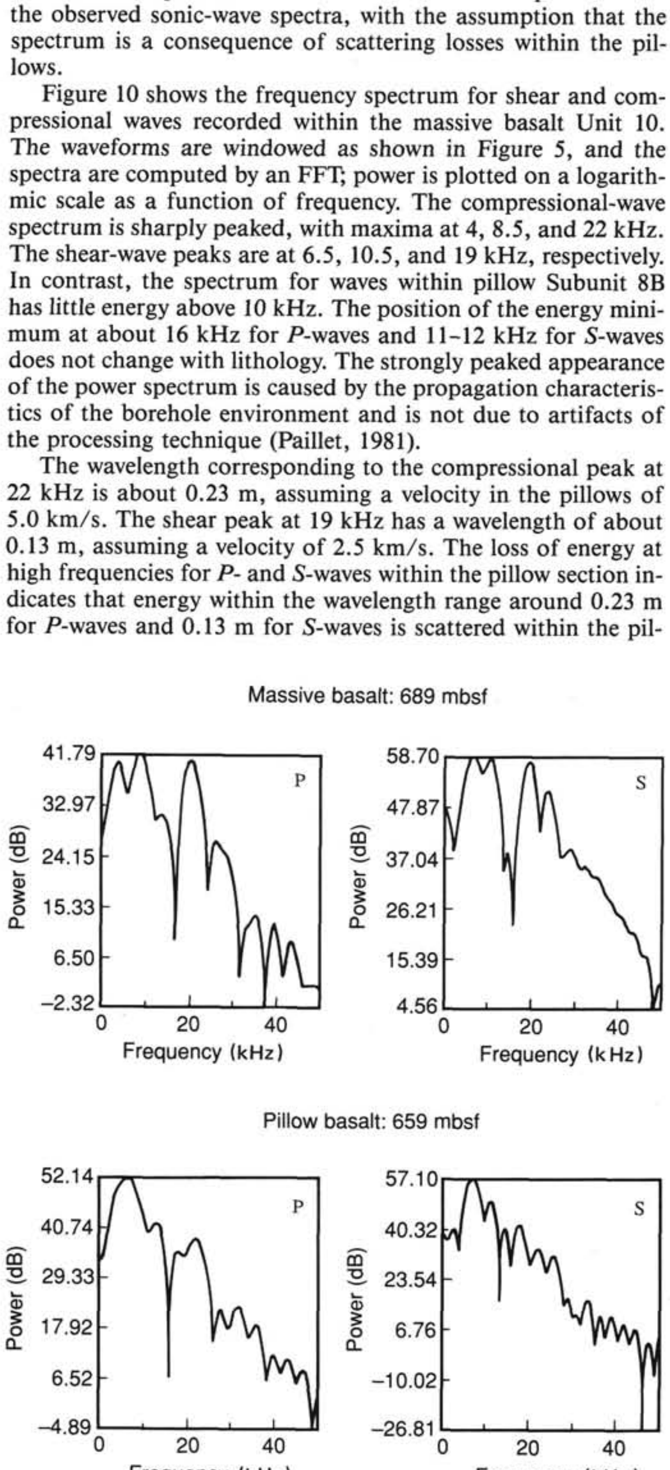

Figure 10. Spectra, showing power in decibels as a function of frequency, of windowed waveforms within massive basalt Unit 10 at 689 mbsf and pillow Subunit 8B at 659 mbsf. The sharp peaks are caused by tuning effects within the wellbore. Note the presence of a peak at about 20 kHz in both the compressional (*P*) and the shear (*S*) arrival within the massive unit not present in the data recorded within the pillows.

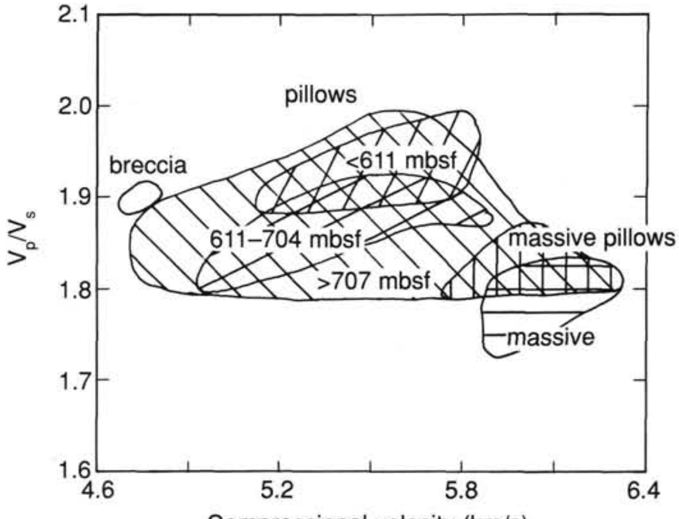

Figure 11. V_p vs. V_p/V_s for Hole 418A by lithology. Shaded areas correspond to the range of data values within each structural type. Shown here are pillows within three depth ranges, massive basalts, massive pillows, and breccias. Data are plotted only if shear and compressional semblance are both above 0.4.

semblance discriminator eliminates more data in the shallower portions of the well, tending to obscure any velocity increase. V_p/V_s is highest in the shallowest pillows (above 1.9) and has intermediate values in the deeper interval. The deepest interval has the lowest V_p/V_s, although the range still includes values above 2.0. The high-velocity "tail" in the pillow field may correspond to short intervals of massive pillows not identified in the core. Within each structural type V_p/V_s appears to increase with increasing V_p.

According to effective-medium theories of wave propagation (e.g., O'Connell and Budiansky, 1974), differences in lithology such as variations in the size of pillows (or even the difference between massive and pillow units) should not greatly affect the velocity ratio because the sonic wavelength is similar to the size of the pillows. In this well, however, the velocity ratio is lowest in massive units and highest in the pillows, as was also observed in DSDP Hole 504B (Moos et al., 1985a). This could perhaps be explained by differences in the properties (such as porosity or pore aspect ratio) of the matrix basalt between pillows and massive units. However, no clear, systematic relationship between velocities and rock type is discernable in core measurements of compressional velocity (see the synopsis in Broglia and Moos, this volume). Salisbury et al. (1985) measured the compressional and shear velocities of over 100 samples from DSDP Hole 504B. They similarly did not observe any systematic difference in V_p or V_s between pillows and flows.

Let us assume that these materials can be modeled using effective-medium theories (e.g., O'Connell and Budiansky, 1974; Kuster and Toksöz, 1974). These theories adequately explain the result that velocities are highest and V_p/V_s is lowest in the uncracked massive units, compared to the pillows and breccias. However, the difference between the properties of the breccia and the pillows cannot be explained by differences in crack distribution. Broglia and Moos (this volume) found anomalously low densities, high porosities, and high potassium content in the breccia, compared to pillows deeper in the well, suggesting that crack porosity is higher and that the cracks are partially filled with alteration products. Replacing fluids in the cracks with stiffer materials will increase V_s more than V_p; thus, the lower V_p and lower ratio in the breccia are explained by a larger number of alteration-filled cracks, in comparison to the pillows. Observations of the cores tend to confirm this result. Unfortunately, velocity data above the Subunit 6A breccia, where the pillows contain large amounts of alteration products, are less reliable due to low semblances (Fig. 8).

Perhaps the most intriguing observation is that V_p/V_s increases with V_p within each depth interval in the pillows. This requires a change in crack aspect ratio to thinner cracks, in combination with a decrease in crack porosity. Alternatively, this requires a decrease in the amount of alteration products within the cracks, combined with a decrease in the crack porosity. This is perhaps a more reasonable explanation. Compressional velocity decreases and porosity increases with alteration in the cores (as discussed by Broglia and Moos, this volume, on the basis of shipboard core measurements). This is consistent with the log velocity data and, furthermore, suggests that variations in both alteration and porosity control the elastic properties of these materials.

Stoneley waves are particularly sensitive to borehole wall permeability (Hsui et al., 1985) and roughness. Both the velocity and energy of this phase are affected. Previous results have revealed a strong dependence of Stoneley energy on fracturing in hard rocks (Paillet, 1983; Moos and Zoback, 1983). The results presented here indicate that similar effects occur in Hole 418A. If the coherence of the Stoneley wave (which is a more direct measure of the amplitude of this phase than a simple energy calculation) is dependent on permeability, then the Stoneley semblance log should reveal the location of permeable intervals within the basaltic section. Looking at the data in Figures 8 and 9 with this in mind, permeable intervals seem to be concentrated at specific points within the section, rather than being distributed throughout, say, the pillow units. For instance, the interval from 479–484 mbsf, breccia Subunit 6A (509–519 mbsf), narrow zones centered at 599 and 624 mbsf, the broad zone from 659–679 mbsf, and narrow intervals at 709 and 759 mbsf all have lower Stoneley semblance. By inference, then, these zones are all potential aquifers. Interestingly, these zones also tend to be zones of lower than normal core recovery or are zones with greater visible alteration. The neutron log records greater porosities within these intervals (Broglia and Moos, this volume).

Correlations between fracturing and waveform distortion measured by semblance have been observed previously by Moos et al. (1985b) and Goldberg et al. (1984). Those studies concentrated on the refracted arrivals. The new results presented here are the first direct quantitative observation of Stoneley-wave distortion in oceanic basalts. Unfortunately, there are no permeability measurements with which these data can be compared, so the above discussion must remain largely speculative.

Although these intervals of low Stoneley semblance do not correspond with unit boundaries, it is interesting to speculate that their properties may be a consequence of conditions during emplacement. For example, Mathews et al. (1984) commented on the systematic variation of log properties within individual units in DSDP Hole 395A. The uppermost sections of each unit had lower resistivities and densities, suggesting higher porosities. Similar results were seen in the log data from ODP Leg 109 (Moos et al., 1986). Perhaps the above intervals identified within DSDP Hole 418A are similar—the uppermost exposed rubbly sections of individual pillow units that were not uniquely identified on the basis of their core properties were therefore systematically under-represented in the recovered analyses.

SUMMARY AND CONCLUSIONS

Twelve-channel full-waveform logs recorded throughout the lowermost 330 m of DSDP Hole 418A during ODP Leg 102 have been analyzed to determine compressional and shear velocities, energies, and frequency contents. Stoneley velocity and coherence were also determined. The average physical properties determined from this analysis are $V_p = 5.5$ km/s, $V_s = 2.9$ km/s, and $V_p/V_s = 1.89$. These values indicate that the section contains a significant number of open cracks, which result in higher V_p/V_s ratios than for intact rocks. Pillows have quite variable velocities and V_p/V_s above 1.8. Massive units have the lowest V_p/V_s and higher velocities than the pillows. One thick breccia unit has lower velocities and V_p/V_s of 1.9. These variations cannot be explained solely on the basis of variations in crack aspect ratio and distribution. Changes in the amount of alteration also play an important role in controlling the elastic properties. Small, stepwise increases in velocity are observed across a major lithologic boundary marked by breccia Subunit 6A, and again at the top of pillow basalt Subunit 13B. Otherwise, velocities are largely independent of depth.

Stoneley velocities increase sharply within the uppermost 100 m of the logged section and are relatively constant in the lowermost 230 m. Increases in Stoneley velocity are observed in massive units, and in fact, this parameter tracks the compressional velocity quite well throughout the logged interval. Stoneley semblance is sharply lower in discrete zones throughout the interval, roughly correlatable to zones of low core recovery and higher neutron porosity. Theoretical considerations suggest that these reductions may indicate zones of high permeability (the tops of individual pillow units?). If this is the case then the lower recovery within these zones implies that aquifers may be under-represented in recovered core. Furthermore, and more importantly, this observation implies that fluid flow through Layer 2 may be concentrated within narrow, well-defined zones, rather than being distributed across entire units. This conclusion can be tested by careful permeability measurements of intervals shorter than those previously tested.

ACKNOWLEDGMENTS

I would like to thank Glen Foss of the Ocean Drilling Program and the Captain and crew of the *JOIDES Resolution* for their assistance during data acquisition. Ken Peters and Divyang Shah assisted in the coding of data acquisition and analysis programs, and David Goldberg also programmed some of the analyses. Discussions with numerous persons, including David Goldberg, Cristina Broglia, Roger Anderson, and Philippe Pezard, provided valuable insights. This work was supported by NSF under JOI-66-84 and OCE-8704609.

REFERENCES

Aki, K., and Richards, P. G., 1980. *Quantitative Seismology Theory and Methods*: San Francisco (W. H. Freeman).

Anderson, R. N., O'Malley, H., and Newmark, R. L., 1985. Use of geophysical logs for quantitative determination of fracturing, alteration, and lithostratigraphy in the upper oceanic crust, Deep Sea Drilling Project Holes 504B and 556. *In* Anderson, R. N., Honnorez, J., Becker, K., et al., *Init. Repts. DSDP*, 83: Washington (U.S. Govt. Printing Office), 443–478.

Anderson, R. N., and Zoback, M. D., 1983. The implications of fracture and void distribution from borehole televiewer imagery for the seismic velocity of the upper oceanic crust at Deep Sea Drilling Project Holes 501 and 504B. *In* Cann, J. R., Langseth, M. G., Honnorez, J., Von Herzen, R. P., White, S. M., et al., *Init. Repts. DSDP*, 69: Washington (U.S. Govt. Printing Office), 255–270.

Cheng, C. H., and Toksöz, M. N., 1981. Elastic-wave propagation in a fluid-filled borehole and synthetic acoustic logs. *Geophysics*, 86: 1042–1053.

Donnelly, T., Francheteau, J., Bryan, W., Robinson, P., Flower, M., Salisbury, M., et al., 1980. *Init. Repts. DSDP*, 51, 52, 53, Pt. 2: Washington (U.S. Govt. Printing Office).

Frankel, A., and Clayton, R. W., 1986. Finite difference simulations of seismic scattering: Implications for the propagation of short-period seismic waves in the crust and models for crustal heterogeneity. *J. Geophys. Res.*, 91:6465–6489.

Goldberg, D. S., Gant, W. T., Seigfried, R. W., and Castagna, J. P., 1984. Processing and interpretation of sonic log waveforms: a case study. *SEG 54th Ann. Symp. (Trans.)*, 28–31.

Han, D., Nur, A., and Morgan, D., 1986. Effects of porosity and clay content on wave velocities in sandstones. *Geophysics*, 51:2093–2107.

Hickman, S. H., Svitek, J. F., and Langseth, M. G., 1984. Borehole televiewer log of Hole 395A. *In* Hyndman, R. D., Salisbury, M. H., et al., *Init. Repts. DSDP*, 78B: Washington (U.S. Govt. Printing Office), 709–716.

Houtz, R., and Ewing, J., 1976. Upper crustal structure as a function of plate age. *J. Geophys. Res.*, 81:2490–2498.

Hsui, T. H., Jinzhong, Z., Cheng, C. H., and Toksöz, M. N., 1985. Tube wave attenuation and in-situ permeability. *Trans. SPWLA Annu. Logging Symp.*, 26:Pap. CC.

Hyndman, R. D., Christensen, N. I., and Drury, M. J., 1984. The physical properties of basalt core samples from Deep Sea Drilling Project Leg 78B Hole 395A. *In* Hyndman, R. D., Salisbury, M. H., et al., *Init. Repts. DSDP*, 78B: Washington (U.S. Govt. Printing Office), 801–810.

Kikuchi, M., 1981. Dispersion and attenuation of elastic waves due to multiple scattering from cracks. *Phys. Earth Planet. Inter.*, 21:159–162.

Kimball, C. V., and Marzetta, T. L., 1984. Semblance processing of borehole acoustic array data. *Geophysics*, 49:274–281.

Kuster, G. T., and Toksöz, M. N., 1974. Velocity and attenuation of seismic waves in two-phase media: Pt. 1. Theoretical formulation. *Geophysics*, 39:587–606.

Little, S. A., and Stephen, R. A., 1985. Costa Rica Rift borehole seismic experiment, Deep Sea Drilling Project Hole 504B, Leg 83. *In* Anderson, R. N., Honnorez, J., Becker, K., et al., *Init. Repts. DSDP*, 83: Washington (U.S. Govt. Printing Office), 517–528.

Mathews, M., Salisbury, M. H., and Hyndman, R., 1984. Basement logging on the Mid-Atlantic Ridge, Deep Sea Drilling Project Hole 395A. *In* Hyndman, R. D., Salisbury, M. H., et al., *Init. Repts. DSDP*, 78B: Washington (U.S. Govt. Printing Office), 717–730.

Mavko, G. M., and Nur, A., 1978. The effect of non-elliptical cracks on the compressibility of rocks. *J. Geophys. Res.*, 83:4459–4468.

Moos, D., Becker, K., and the Leg 109 Shipboard Party, 1986. Physical properties of young oceanic crust from geophysical logs in DSDP Hole 395A. *Eos, Trans. Am. Geophys. Union*, 67:1213. (Abstract)

Moos, D., Goldberg, D., Hobart, M. A., and Anderson, R. N., 1985a. Elastic-wave velocities in Layer 2A from full waveform sonic logs at Hole 504B. *In* Leinen, M., Rea, D. K., et al., *Init. Repts. DSDP*, 92: Washington (U.S. Govt. Printing Office), 563–570.

Moos, D., Goldberg, D., and Zoback, M. D., 1985b. Velocity and natural fracturing at the Kent Cliffs well, Peekskill, NY. *Eos, Trans. Am. Geophys. Union*, 66:363. (Abstract)

Moos, D., and Zoback, M. D., 1983. *In situ* studies of velocity in fractured crystalline rocks. *J. Geophys. Res.*, 88:2345–2358.

Newmark, R. L., Anderson, R. N., Moos, D., and Zoback, M. D., 1985. Sonic and ultrasonic logging of Hole 504B and its implications for the structure, porosity and stress regime of the upper 1 km of the oceanic crust. *In* Anderson, R. N., Honnorez, J., Becker, K., et al., *Init. Repts. DSDP*, 83: Washington (U.S. Govt. Printing Office), 479–510.

O'Connell, R. J., and Budiansky, B., 1974. Seismic velocities in dry and saturated cracked solids. *J. Geophys. Res.*, 79:5412–5423.

Paillet, F. L., 1981. Predicting the frequency content of acoustic waveforms obtained in boreholes. *Trans. SPWLA Annu. Logging Symp.*, 22:Pap. I.

________, 1983. Acoustic characterization of fracture permeability at Chalk River, Ontario, Canada. *Can. Geotech. J.*, 20:468–476.

Paillet, F. L., and White, J. E., 1982. Acoustic modes of propagation in the borehole and their relationship to rock properties. *Geophysics*, 47:1215–1228.

Rosenbaum, J. H., 1974. Synthetic microseismograms: logging in porous formations. *Geophysics*, 39:14–32.

Salisbury, M. H., Christensen, N. I., Becker, K., and Moos, D., 1985. The velocity structure of Layer 2 at Deep Sea Drilling Project Site 504 from logging and laboratory experiments. *In* Anderson, R. N., Honnorez, J., and Becker, K., et al., *Init. Repts. DSDP*, 83: Washington (U.S. Govt. Printing Office), 529–539.

Salisbury, M., Stephen, R., Christensen, N. I., Francheteau, J., Hamano, Y., Hobart, M., and Johnson, D., 1980. The physical state of the upper levels of Cretaceous oceanic crust from the results of logging, laboratory studies, and the oblique seismic experiment at Deep Sea Drilling Project Sites 417 and 418. *In* Donnelly, T., Francheteau, J., Bryan, W., Robinson, P., Flower, M., Salisbury, M., et al., *Init. Repts. DSDP*, 51, 52, 53, Pt. 2: Washington (U.S. Govt. Printing Office), 1579–1597.

Wu, T. T., 1966. The effect of inclusion shape on the elastic moduli of a two-phase material. *Int. J. Solids Struct.*, 2:1–8.

Wyllie, M.R.J., Gregory, A. R., and Gardner, G.H.F., 1958. An experimental investigation of the factors affecting elastic wave velocities in porous media. *Geophysics*, 23:459–493.

Date of initial receipt: 5 March 1987
Date of acceptance: 9 October 1987
Ms 102B-114